Mechanical and microstructural properties of nitinol fabricated on a preheated Ti6Al4V base plate using laser direct metal deposition (LDMD) process

Samuel Skhosane[1] , *Nthabiseng* Maledi[2*] & *Sisa* Pityana[1, 3]

[1]Manufacturing Cluster, Photonics Centre, Council for Scientific and Industrial Research, Pretoria, South Africa
[2]School of Chemical and Metallurgical Engineering, University of the Witwatersrand, Private Bag 3, Wits, 2050, South Africa
[3]Department of Chemical and Metallurgical Engineering, Tshwane University of Technology, Pretoria, South Africa

Abstract. This study reports the microstructure and mechanical properties of Nitinol fabricated on a pre-heated Ti6Al4V plate using laser direct metal deposition (LDMD). Commercial nitinol powder with approximately 50:50 wt.% ratio of nickel to titanium was laser deposited on a preheated Ti6Al4V plate. The produced samples were characterized using optical microscopy (OM), scanning electron microscopy (SEM), and Vickers hardness tester. The hardness was measured transversely on the deposited layers. The hardness obtained on the pre-heated substrate remained uniform with an increase in linear energy density. However, on a non-preheated substrate, the hardness decreased as the linear energy density increased.

1 Introduction

Nitinol or titanium alloy comprises approximately 50:50 wt.% ratio of titanium (Ti) and nickel (Ni) mainly known within the biomedical field, it is popular because of possessing two fascinating properties: the ability to return to its original shape after being deformed (shape memory effect) and superelasticity [1, 2].

The choice of nitinol amongst many materials to be used within biomedical relies on its transition temperatures that are much closer to or below the normal body temperature [3]. The overall intention of selecting nitinol alloy is mainly based on seeking superelasticity or shape memory effect properties. When the austenite(B2) transition temperature is below the body temperature, then the shape memory effect is used for its superelasticity and when the body temperature is below martensitic(B19) then the shape memory alloy is used for its shape memory effect [3].

Nickel is a major alloying element in NiTi. However, nickel is known to be a toxic material that causes allergies, but when paired with titanium at an approximately equal atomic ratio, its toxicity is not seen since titanium produces a layer that prevents direct contact of nickel to the body [3].

The use of nitinol material for manufacturing implants and stents within the medical field has surpassed the use of stainless steel because nitinol has good biocompatibility [7], and low elasticity [4]. However, a slight change in nickel composition changes the austenite-to-martensitic temperature affecting superelasticity and the shape memory effect properties [4].

Casting and powder metallurgy are the known traditional routes for manufacturing nitinol components [5]. However, globally, the manufacturing industry is gradually adopting additive manufacturing (AM) technology. AM is popular in producing complex shapes [5, 8, 9]. One of the famous AM processes is laser direct metal deposition (LDMD) also known by other names such as direct energy deposition (DED), laser metal deposition (LMD), and laser engineer net shaping (LENS) [9]. Laser direct metal deposition (LDMD) can be used for 3-D printing or laser cladding. The effectiveness of the LDMD process relies on getting the optimum parameters that can yield a defect-free product. Several variables to consider in achieving a good structure include laser power, laser scanning speed, laser beam diameter, powder feed rate, hatch spacing or overlap percentage, cooling rate, and shielding gas. However, most studies consider using linear energy density which accounts for laser power and laser scanning speed at a fixed laser beam diameter and fixed rate of filler material as shown in Equation 1 [9, 10, 11].

$$Linear\ energy\ density, E = \frac{Laser\ power(P)}{Laser\ scanning\ speed(V)} \quad \text{............... Equation (1)[11]}$$

Laser AM process yields fine grain structure due to rapid solidification, however, processing crack-sensitive material has cracking issues because of stress induced by fast solidification [11].

Biomedical implant components are of highly complex shapes and have austenitic superelasticity properties [4]. Superelasticity is an elastic response of a material that is loaded or stressed to recover its original shapes after being unloaded, this superelasticity property in NiTi is very important for biomedical implants to avoid permanent failure, however, fabrication of implants using AM process yields higher hardness as compared to as-cast due to fast cooling associated with this process [6], therefore, nitinol components produced via the AM process are brittle and difficult to machine.

On the other hand, the use of traditional processes such as casting and sintering also comes with post-processing (stress relieving, annealing normalizing) costs and high costs of discarded material during machining. The as-cast-produced nitinol has a lower hardness after post-heat treatment in the range of 340-440Hv [12] while the hardness of the as-produced 3D printed via selective laser melting (SLM) process ranges from 540-735Hv [6].

Sharma et al. [5] investigated the microstructure and mechanical properties of nitinol fabricated using the DED process, and the hardness of the clad at the bottom, middle, and top zones measured 263Hv, 303.7Hv and 240Hv respectively. Higher hardness measured in the middle of the clads was due to the precipitation of Ni_4Ti_3. The precipitation of Ni_4Ti_3 was associated with the reheating of the underneath layer. Ni_4Ti_3 precipitates along the grain boundaries, it then acts as a barrier for dislocation and results in increasing superelasticity and hardness. The selective laser melting (SLM) AM process yields higher hardness as compared to the DED process [6].

Ghosal et al. [9] studied the DED process and focused on finding a proper setup configuration that can help achieve high-quality deposition, it was confirmed that DED produces metallurgical bonding on the base, however, the parts produced from DED still require polishing or machine finishing.

In this study, the investigation focuses on investigating the influence of preheating on the microstructure of nitinol produced using the AM process called the LDMD process. The investigation aims to use preheating to reduce solidification rates and consequently reduce the hardness that is due to the formation of the martensitic structure and the intermetallic phase. The importance of reducing hardness is associated with improvement in machinability and improvement in fatigue properties.

2 Methodology

2.1 Material

Pre-alloyed commercial nitinol powder supplied by Wear Tech (Pty) (LTD) with a particle size distribution of 45-90 µm was used as a feedstock material. The material composition as per the supplier`s certificate is shown in Table 1

Table 1. Nitinol chemical composition

Element chemical formula	Ni	Ti	Fe	C	O	N
Weight percent (wt.%)	55.78	Balance	0.01	0.011	00059	0.005

Fig.1 presents scanning electron microscope (SEM) micrographs of powder morphology and energy dispersive spectroscopy (EDS) analysis of the gas-atomized nitinol powder. The powder distribution and chemical composition were measured using JEOL JSM 6510 (SEM) with energy dispersive spectroscopy (EDS.

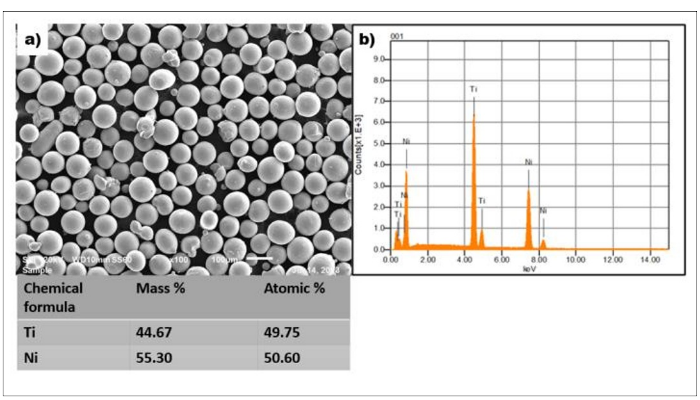

Fig. 1. (a) Nitinol SEM morphology and (b) EdX analysis.

Fig.1(a) shows the SEM image with evidence of spherical particles. The EDX analysis shown in Fig.1(b) confirms that the powder contains approximately equal atomic percent of Ni: T.

2.2 Process parameters

Laser deposition of nitinol clads was performed on both preheated and non-preheated 6×100×100mm Ti6Al4V plate using IPG fibre laser that uses 1073 wavelength. The scanning of the powder jet from the powder feeder through a 3-way nozzle mounted on a Kuka robot machine was melted using a 2mm laser beam diameter. Layer-by-layer laser cladding at 50% overlapping using a zigzag strategy was used in building samples of approximately 40 ×6 ×6 mm in size.

This study assumed linear energy density reflecting a combination effect of laser power and laser scanning speed as the main parameter as used by previous authors in Equation 1. The laser beam diameter, powder feed, and argon shielding gas flow rate were fixed at 2 mm, 2 rpm, and 15 l/min respectively. Before laser deposition, the Ti6Al4V base plates were first sandblasted to remove contamination, then preheated to temperatures between 250°C and 300°C on a heating stage using the heating stage furnace, and a pyrometer was used to measure the base plate temperature.

Table 2. Laser parameters process optimization.

Pre-heated	Non-preheated	Laser Power(W)	Laser Scanning speed(m/s)	Linear Energy density (KJ/m)
a	**f**	1200	0.025	48.00
b	**g**	1200	0.020	60.00
c	**h**	1100	0.015	73.33
d	**i**	1200	0.015	80.00
e	**j**	1300	0.015	86.66

2.3 Metallographic preparation and characterization

Metallographic samples were sectioned across the laser cladding direction using a bend saw cutting machine. In the first stage, sectioned samples were mounted using a black resin. In the second stage, the samples were ground down to level, to smoothen the surface and to remove burrs from the cutting medium.

The 240, 320, 600, 800 to 1200 grits paper sizes were sequentially used for grinding samples. Ground samples were polished to mirror surface finish of 0.04 µm using the Med-Chem polishing cloth and diamond suspension liquid ranging from 9 µm, 6 µm, 3 µm, and 0.04 µm. Polished samples were etched using Kroll's reagent (6 ml nitric acid, 2 ml hydrofluoric acid, and 92 ml distilled water) by immersing the samples for approximately 10 seconds.

Olympus BX51M Optical Microscope (OM) and Jeol JSM 6510 SEM with energy dispersive spectroscopy (EDS) were used for microstructural analysis.

2.4 Mechanical testing

The hardness was evaluated by using Zwick Vickers microhardness machine. The indentations were performed at a load of 500 g, a dwell time of 10 sec with the spacing between the indentations kept at 600 µm. About 8 indentations were performed in the transverse direction from top to bottom sectioned clad.

2.5 X-ray diffraction (XRD)

X-ray diffraction (XRD) (XPERT PRO Analytical Netherland) was used to determine the phases present in preheated and non-preheated clads. Cu kα radiation (ƛ = 0.1545 nm) was used with the voltage and current settings at 45 kV and 40 mA respectively. The X-ray patterns were scanned over a 2θ ranging from 10°- 90°. XPert High score software was used to analyse the patterns obtained from the XRD scans.

3 Results

3.1 Optical micrographs of both preheated and non-preheated nitinol

Fig.2 presents the optical micrographs of NiTi clads produced on preheated and non-preheated clads Ti6Al4V base, the micrographs were taken from the top of the clads, Fig.2(a-e), represent the preheated in order of increasing linear energy density same Fig.2(f-j) represents the non-preheated nitinol clads in order of increasing linear energy density.

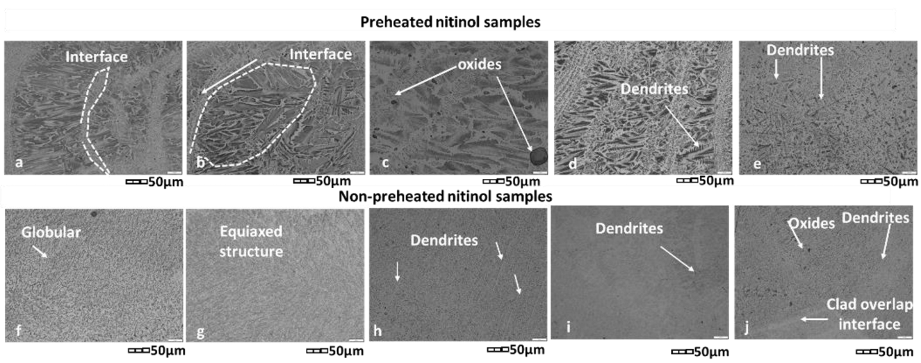

Fig. 2. (a-e) Optical micrographs of preheated (a-e) and non-preheated (f-j) nitinol samples

Fig.2(a-d) micrographs for the preheated clad show elongated grains perpendicular to the clad fusion interface area circled in a white dotted line, while Fig.2(e) fabricated at higher linear energy density shows finer dendrites mixed with fine irregular global shape structure.

Fig.2(f) micrographs show fine globular structure, Fig.2(g) micrographs show equiaxed and globular structure while Fig.2(h, i & j) show dendritic structure. For the non-preheated nitinol, globular was associated with fast cooling while the dendritic structure was because of an increase in heat input as linear energy density increases. The microstructure of both preheated and non-preheated clads had no pores and were crack-free, however, oxides were observed on preheated samples.

3.2 SEM results

Fig.3 presents the SEM micrographs of nitinol clads produced from preheated and non-preheated Ti6Al4V base plates. The microstructural observations were taken from the top and the bottom interphase of clads and presented in the order of increase in linear energy density. The micrographs are comprised of black phase, a light grey phase and white precipitates on the boundaries of the light grey phase.

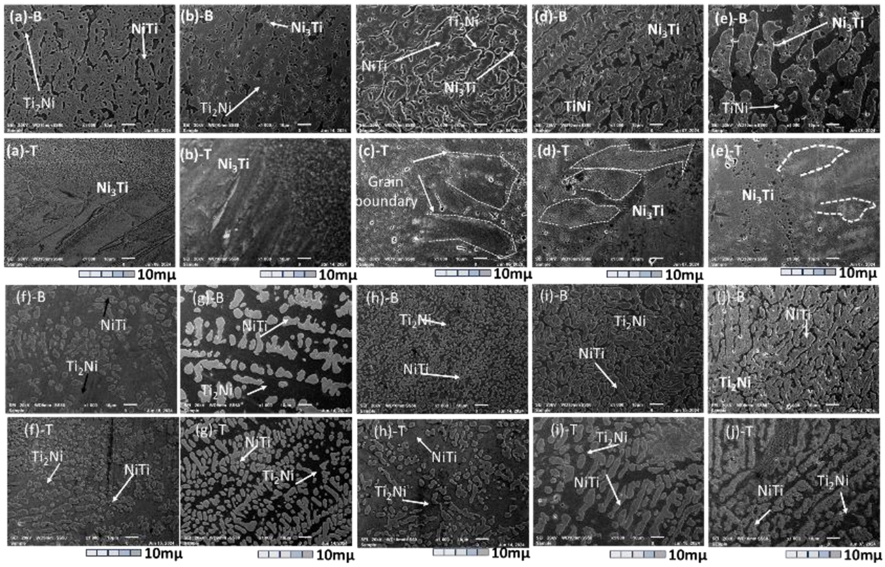

Fig. 3. SEM micrographs of the bottom section of the preheated samples (a-e) denoted B, the top section of the preheated samples (a-e) denoted T, the bottom section of non-preheated samples (f-j) denoted B, and top section of non-preheated samples (f-j) denoted T. Grain boundaries and sub-grains are circled by white dotted lines.

The SEM-EDX analysis of preheated samples Fig.3(a-e) shows the black matrix rich in titanium (Ti) composition, which was attributed to the Ti_2Ni intermetallic phase, while the light grey phase with the composition of approximately 50:50 ratio between Ni:Ti was attributed to NiTi compound. The white strips and spots are rich in nickel (Ni) and were attributed to Ni_3Ti. Fig.3(a-e) shows an increase in the black phase with an increase in energy density. The top microstructure of Fig.3(a-e) shows elongated grains circled in a white dotted line. Fig.3(e) shows nucleation of dendritic sub-grain.

The non-preheated samples Fig.3(f-j) also show a black matrix which denotes to Ti_2Ni and a grey phase which attributes to NiTi. The Ti_2Ni intermetallic phase found in non-preheated samples increased with increasing linear energy density.

3.3 XRD results

Fig.4 presents the XRD patterns of the nitinol clads samples produced via the LDMD process depositing nitinol powder on preheated and non-preheated Ti6Al4V bases. The XRD analysis was only performed on samples “b” and “g” due to financial constraints.

 https://doi.org/10.1051/matecconf/202440607006

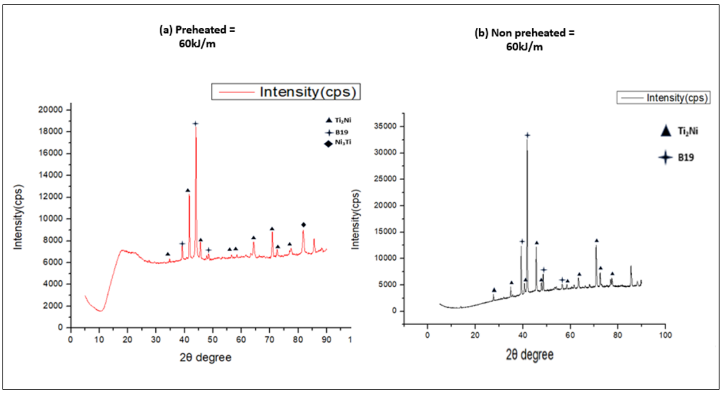

Fig. 4. (a) XRD patterns of the preheated and (b) non-preheated nitinol samples produced via the LDMD process

Based on the XRD patterns for both preheated and non-preheated as shown in Fig.4, there is predominant evidence of martensitic phase(B19) with some Ti_2Ni intermetallic (PDF JCPDS Nr 18-0899, Nr. 35-1281, Nr.72-0442 and Nr. 75-0878). However, the Ni_3Ti intermetallic phase was identified in the preheated sample Fig.4(a).

3.4 Hardness results

Fig.5 presents the Vickers hardness measurements of clads produced from preheated Ti6Al4V base plates. The hardness measurements were taken transverse to the clad length and repeated 3 times at different areas.

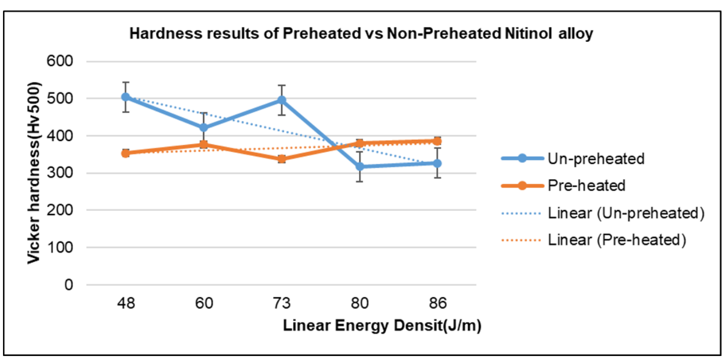

Fig. 5. Vickers hardness of the preheated and non-preheated nitinol samples.

The comparison of hardness results of preheated and un-preheated nitinol samples produced with varying linear energy densities is shown in Fig.5. From the figure, it can be seen that the hardness values of preheated samples were nearly constant. However, sample c which was produced at 73J/m reported a slightly lower hardness.

The hardness of un-preheated samples decreased with increasing linear energy density. The un-preheated sample h was an outlier and did not follow a similar trend. The hardness of the sample was slightly higher than the rest of the samples.

Low hardness values of preheated samples at 48J/m, 60 J/m, and 73 J/m energy densities were attributed to slow solidification rates and softening due to grain growth as observed in SEM micrographs in Fig 3 (a-f). High hardness values of un-preheated samples were because of rapid solidification rates, which led to the formation of finer dendritic microstructures.

However, at higher linear energy densities (i.e. 80J/m and 86 J/m) the hardness dropped below the hardness values of preheated samples.

4 Discussion

4.1 Influence of preheat on microstructure

Optical microstructures of preheated samples shown in Fig.2(a-d) showed elongated grains in the build direction. However, Fig.2 (e) shows a mixture of both dendritic and globular microstructure. The observed larger grains were due to high heat inputs. Preheating assisted in retarding the cooling rate, subsequently softening and homogenizing the microstructure. The hardness of the preheated samples was expected to be lower than that of non-preheated samples due to the grain growth observed on preheated samples.

The non-preheated samples Fig.2(f) showed fine globular structure, which was due to rapid cooling, Fig.2(g) shows a mixture of fine globular and equiaxed structure while Fig.2(h, i &j) indicate a large dendritic and globular structure in all areas which confirms the effect of slow solidification of laser processing [11].

SEM results presented in Fig.3 are for both preheated and non-preheated samples. The main phases observed were the NiTi matrix and Ti_2Ni intermetallic, However, the preheated sample showed additional white precipitate surrounding the NiTi phase rich in nickel. The precipitates were attributed to Ni_3Ti. According to the Ni-Ti phase diagram, Ni_3Ti forms from the nickel-rich composition [13]. Thus, it can be assumed that the introduction of the preheat led to the reduction of titanium composition, due to the oxidation of Ti. The small drift in chemical composition affects the thermal transition temperature [10].

The XRD patterns of the non-preheated sample (Fig 4 (b) reported high intensity of the martensitic B19, whereas the XRD pattern in Fig.(4a) for the preheated sample reported half the intensity at the same angle. It was assumed that a higher intensity of B19 reported in non-preheated was associated with rapid cooling rates which produce very hard B19 phase. Fast cooling yields higher hardness because the base acts as a heat sink [5].

The XRD results also confirmed the evidence of Ni_3Ti in the preheated sample, which is evidence of equilibrium solidification within Ni-rich nitinol. The precipitation of Ni_3Ti intermetallic along grain boundaries prohibits dislocation movement during mechanical deformation, thus leading to precipitation hardening [13].

4.2 Influence of preheating on hardness

Assessment of hardness for the non-preheated sample in Fig.5 shows a slight decrease in hardness as the linear energy density increases. However, increasing linear energy density decreases the solidification rate which yields grain growth and results in lowering the hardness.

The hardness of the preheated nitinol samples shows slightly lower hardness than non-preheated samples. Therefore, it can be concluded that preheating resulted in decreasing the hardness by reducing the solidification rates. In addition, the hardness of preheated samples was almost similar when linear energy densities were varied, clearly showing that the samples were homogenized. A decrease in hardness for the preheated nitinol alloy was associated with softening of the martensitic structure. The decrease in hardness could be beneficial for mechanical properties and better machining. The hardness of the non-preheated samples at higher linear energy density shows lower hardness, again, it can be concluded that high heat input slows the solidification rates resulting in reducing the hardness.

5 Conclusion

The study used a non-preheated and a preheated Ti6Al4V base plate to produce laser deposited nitinol samples under varying linear energy densities. The investigation was intended to study the effect of preheating on the microstructure and mechanical properties of nitinol, with the expectation of lowering the hardness since additive manufacturing of nitinol is known to produce hard microstructure that is difficult to machine. The following findings were made from the study:

- The preheated nitinol samples at a temperature between 250°C and 300°C yielded two microstructures at the top and bottom of the produced samples. The top sample was comprised of perpendicular elongated grains, whilst the bottom interphase yielded a mixture of dendrites and globular structure.
- The SEM micrographs of both preheated and non-preheated samples reported a high proportion of B19 Ti_2Ni. The preheated samples also reported Ni_3Ti.
- The XRD pattern detected B19, Ti_2Ni and Ti_3Ni, however, no B2 phase detected.
- Preheated nitinol samples reported homogenized hardness lower than that of non-preheated samples. In addition, the non-preheated samples reported a decrease in hardness with an increase in linear energy density.
- The preheated sample produced at 73J/m was regarded as the best sample due to lower hardness as compared to non-preheated. This hardness is lower than the as-produced SLM nitinol and in a range of the as-cast nitinol post-processed nitinol.

The authors appreciated acknowledged and thanked the contributions of funding from the National Research Council (NRF) through the Thuthuka Funding Programme and the Council for Scientific and Industrial Research (CSIR) for financial and resource support not forgetting CSIR personnel who contributed to this work.

References

1. D. Cascadan, C. Grandini. Adv. Met. Eng. ED. (2019).
2. J. Chekotu, R. Groarke, K. O'Toole, D. Brabazon, Mater.**12.5**, (2019)
3. A. Wadood, Adv. Mater. Sci. Eng. **1**, (2016)
4. P. Jamshidi, C. Panwisawas, E. Langi, S. Cox, J. Feng, L. Zhao and M. Attallah, J. Alloys Compd. **909**, (2022)
5. V. Sharma, D. D. M. Svetlizky, O. Tevet, M. Krämer, S. Kim, B. Gault, N. Eliaz, Addit. Manuf. **86**, (2024)
6. I. Shishkovsky, I. Yadroitsev, I. Smurov. Phys. Procedia. **39** (2012)
7. A. Pelton, D. Stockel, T. Duerig. Mater. Sci. Forum. **327** (2000)
8. M. Attaran, Bus. Horiz*,* **60**, (2017)
9. P. Ghosal, M. Majumder, A. Chattopadhyay, Mater. Today Proc. **5** (2018)
10. A. Baran, M. Polanski, J. Alloys Compd*,* **750**, (2018)
11. J. Zhu, E. Borisov, X. Liang, R. Huizenga, A. Popovich, V. Bliznuk, R. Petrov, M. Hermans, V. Popovich. J. Mater. Sci. **57**, (2022)
12. H. Huang, H. Zheng, G. Lim, Appl. Surf. Sci. **228,** (2004)
13. M. Sathishkumar, C. Kumar, S. Ganesh, M. Venkatesh, N. Radhika, M. Vignesh, A. Pazhani, J. Manuf. Processes, **102**(2023)